AGING DEGRADATION OF CAST STAINLESS STEEL*

O. K. Chopra and H. M. Chung

Materials Science and Technology Division
ARGONNE NATIONAL LABORATORY
Argonne, Illinois 60439

CONF-8510173--25

TI86 003068

October 1985

To be presented at the 13th Water Reactor Safety Research Information Meeting, October 22-25, 1985, National Bureau of Standards (NBS), Gaithersburg, MD.

*Work supported by the Office of Nuclear Regulatory Research, U. S. Nuclear Regulatory Commission, under Contract W-31-109-Eng-38.

AGING DEGRADATION OF CAST STAINLESS STEEL

O. K. Chopra and H. M. Chung

Materials Science and Technology Division
ARGONNE NATIONAL LABORATORY
Argonne, Illinois 60439

Abstract

A program is being conducted to investigate the significance of in-service embrittlement of cast-duplex stainless steels under light-water reactor operating conditions. Data from room-temperature Charpy-impact tests for several heats of cast stainless steel aged up to 10,000 h at 350, 400, and 450°C are presented and compared with results from other studies. Microstructures of cast-duplex stainless steels subjected to long-term aging either in the laboratory or in reactor service have been characterized. The results indicate that at least two processes contribute to the low-temperature embrittlement of duplex stainless steels, viz., weakening of the ferrite/austenite phase boundary by carbide precipitation and embrittlement of ferrite matrix by the formation of additional phases such as G-phase, Type X, or the α' phase. Carbide precipitation has a significant effect on the onset of embrittlement of CF-8 and -8M grades of stainless steels aged at 400 or 450°C. The existing correlations do not accurately represent the embrittlement behavior over the temperature range 300 to 450°C.

1. Introduction

The ferrite phase in the duplex austenitic/ferritic structure of cast stainless steels increases the tensile strength and improves weldability, resistance to stress corrosion, and soundness of casting of these steels. However, various carbide phases, intermetallic compounds such as sigma and chi phase, and the chromium-rich α' phase can precipitate in the ferrite phase during service at elevated temperatures and lead to substantial variations in mechanical properties.[1] It has long been known that ferritic stainless steels are susceptible to severe embrittlement when exposed to temperatures in the range of 300 to 500°C, due to precipitation of the α' phase.[2,3] The potential for significant embrittlement of cast-duplex stainless steels has been confirmed by recent studies on cast materials that were aged at temperatures between 300 and 450°C for times up to 70,000 h (~8 yr).[4-7]

In general, thermal aging of cast-duplex stainless steels at temperatures <450°C causes an increase in hardness and tensile strength and a decrease in ductility, Charpy-impact strength, and J_{IC} fracture toughness of the material. The room-temperature impact energy can be reduced by ~80% after aging

for ~8 yr at temperatures as low as 300°C.[4] The ferrite content of the cast structure has a pronounced influence on the embrittlement behavior, namely, an increase in ferrite increases susceptibility to embrittlement. Most investigations characterize the degree of embrittlement primarily in terms of Charpy-impact energy in notched toughness tests. The fracture mechanics analyses needed to assess the behavior of piping and components under reactor operating conditions require measures of fracture toughness obtained by J-R curve tests. Such toughness measurements have not been carried out on long-term, low-temperature aged material or on material that has actually experienced reactor service.

The current "best estimates" of degree of embrittlement at the operating temperatures of light-water reactors (LWRs), i.e., 280 to 320°C, are obtained from Arrhenius extrapolations of the laboratory data. The aging time to reach a given degree of embrittlement at different temperatures is determined from

$$t = 10^{P} \exp\left[\frac{Q}{R}\left(\frac{1}{T} - \frac{1}{673}\right)\right], \qquad (1)$$

where Q is the activation energy, R the gas constant, T the absolute temperature, and P the aging parameter which represents the degree of aging reached after 10^{P} h at 400°C. The activation energy for the process of embrittlement has been described as a function of chemical composition of the cast material.[7] Thus,

$$Q(\text{kcal/mole}) = -43.64 + 4.76\ (\%\ \text{Si}) + 2.65\ (\%\ \text{Cr}) + 3.44\ (\%\ \text{Mo}). \qquad (2)$$

Chemical compositions of the various cast materials in low-temperature aging studies[4,7] yield activation energies between 15 and 24 kcal/mole for cast CF-8 or CF-3 stainless steels and between 18 and 25 kcal/mole for cast CF-8M stainless steels.

Such an approach is a powerful tool for accelerated testing when it can be clearly established that the same mechanisms are operating over the temperature range involved in the extrapolation. Although the experimental data include a few tests at reactor operating temperatures, most of the work has been conducted at higher temperatures (350 to 450°C), and the validity of extrapolation of these data to lower temperatures needs to be better established.

The available information is not sufficient to determine the mechanism of embrittlement or to correlate the microstructure with mechanical properties. Microstructural studies on several heats of cast-duplex stainless steels that were aged for times up to 70,000 h at 400, 350, and 300°C revealed the formation of the G-phase (a phase rich in Ni and Si) and two other precipitates which were not α'.[8,9] The G-phase and chromium-rich α' phase have been identified by atom probe field-ion microscopy, in another heat of cast-duplex

stainless steel aged for 7500 h at 400°C.[10,11] Furthermore, the data on cast stainless steels aged at temperatures below 450°C yield activation energies well below the 55 kcal/mole value associated with chromium bulk diffusion, the process that has most commonly been assumed to be rate controlling in the low-temperature embrittlement of ferritic steels.

These results indicate differences in the mechanism of embrittlement over the temperature range of 300 to 450°C or processes other than precipitation of additional phases in the ferrite matrix contribute to embrittlement of cast-duplex stainless steels. The time required for embrittlement at reactor operating temperatures preclude direct, conventional, laboratory testing. Instead, microstructural studies and mechanical testing of materials from components that have seen extended field service need to be carried out to ensure that the mechanisms involved in the higher temperature laboratory experiments are the same as those occurring in the reactor.

The objectives of this program are to (1) characterize the microstructure of in-service reactor components and laboratory-aged material, correlate microstructure with loss of fracture toughness, and identify the mechanism of embrittlement; (2) determine the validity of laboratory-induced embrittlement data for predicting the toughness of component materials after long-term aging at reactor operating temperatures; (3) characterize the loss of fracture toughness in terms of fracture mechanics parameters to provide the data needed to assess the safety significance of embrittlement; and (4) provide additional understanding of the effects of key compositional and metallurgical variables on the kinetics and degree of embrittlement.

The relationship between aging time and temperature for onset of embrittlement will be determined by microstructural examination and measurements of hardness, Charpy-impact and tensile strengths, and J_{IC} fracture toughness. Estimates of the degree of embrittlement obtained from laboratory-aged material will be compared with data for material from actual reactor service. The kinetics and fracture toughness data generated in this program and from other sources will provide the technical basis to define the aging histories, chemical compositions, and metallurgical structures that lead to significant embrittlement of cast stainless steels under LWR operating conditions.

2. Material Characterization

Material was obtained from nineteen experimental heats (static-cast keel blocks) and six commercial heats (centrifugally cast pipes and static-cast pump impeller and pump casing ring) of CF-3, -8, and -8M grades of cast-duplex stainless steel. Six of the experimental heats were also procured in the form of 76-mm-thick slabs. Charpy-impact specimen blanks were obtained from all the experimental and commercial heats of material. Blanks for compact tension and tensile specimens were obtained from sections of cast pipes, pump casing ring, pump impeller, and the cast slabs. The specimen blanks are being aged at 450, 400, 350, 320, and 290°C for times up to 50,000 h.

Fractured impact test bars from three heats of aged cast stainless steel, grades CF-8 and -8M, were obtained from the Georg Fischer Co., Switzerland. The materials were used to study the long-term aging behavior of cast stainless steel.[1] The specimens from CF-8 material (Heats 280 and 278) were aged for 3000, 10,000, and 70,000 h at 300, 350, and 400°C, while the specimens from CF-8M material (Heat 286) were aged for 1000 and 10,000 h at 400°C. A cover plate assembly of cast stainless steel from the recirculation pump of the KRB reactor was also procured. The reactor was in service for ~12 yr. The plate assembly was decontaminated and samples were obtained from different sections of the plate for microstructural characterization and mechanical testing.

The chemical composition, ferrite content, hardness, ferrite morphology, and grain structure of the various castings have been reported previously.[12,13] The centrifugally cast pipe material contains equiaxed or radially oriented columnar grains, while the static-cast keel blocks, slabs, and the pump impeller contain a mixed grain structure. The ferrite contents of the cast materials range between 3 and 30%. The ferrite morphology for the castings containing >5% ferrite is either lacy or acicular. A change in the ferrite content of the duplex material has very little effect on the concentrations of Ni and Cr in the two phases. For all materials, some differences in the chemical composition, ferrite content, and hardness are observed for material from the top or bottom region of the static-cast keel blocks and slabs or the inner and outer diameter of the centrifugally cast pipes. In general, the hardness of the cast material increases with an increase in ferrite content. For the same ferrite content, the hardness of CF-8 and -8M material is comparable, while the hardness of CF-3 material is lower. An increase in nitrogen content increases the hardness of all grades of cast stainless steel. Test matrices for the various mechanical tests and the time and temperature of aging for the different cast materials have been reported.[8]

3. Influence of Aging on Charpy-Impact Toughness

Charpy-impact tests were conducted at room temperature on the various heats of material aged up to 10,000 h at 350, 400, and 450°C. Standard Charpy V-notch specimens were machined from the aged and unaged materials according to ASTM specification E-23. A Dynatup Model 8000A drop-weight impact machine with an instrumented tup and data readout system was used for the tests. The data indicate that thermal aging of cast stainless steels with >10% ferrite causes a substantial decrease in impact energy. Materials with >20% ferrite show a drastic reduction in impact energy after aging for ~300 h at 450°C or ~3000 h at 400°C. In general, the low-carbon CF-3 grades of cast stainless steels exhibit greater resistance to embrittlement than do the CF-8 and -8M grades.

Figure 1 shows the load-time curves for Heat 60 in the unaged condition and after aging for 300, 3000, and 10,000 h at 400°C. The results show two important features, namely, thermal aging leads to a reduction in impact energy and an increase in the strain hardening rate of the material. The strain hardening rate increases after aging for a relatively short time (i.e.,

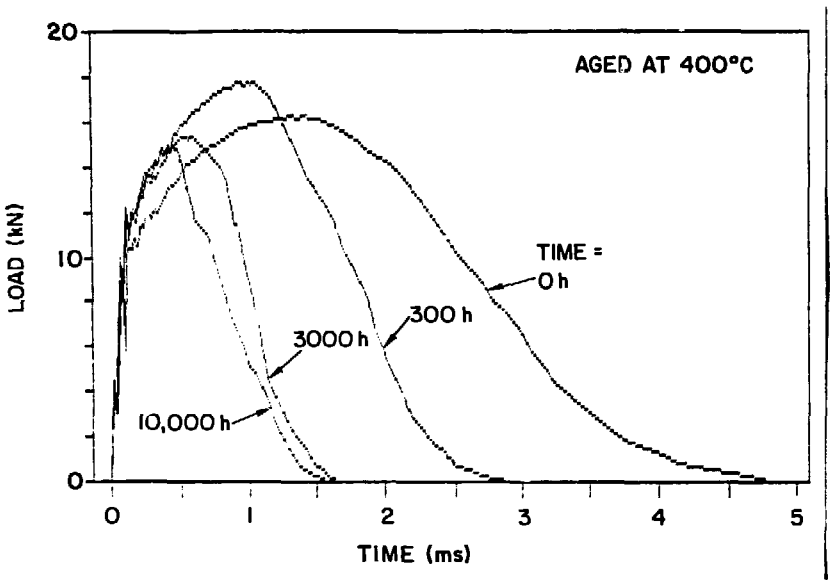

Fig. 1. Load-Time Curves for Charpy V-notch Specimens of Heat 60 Tested at Room Temperature.

~300 h) and does not change significantly with further aging. The maximum load for a specimen that was aged for 300 h is greater than that for the unaged material. The higher strain hardening rates for the aged material are associated with the precipitation reactions in the ferrite matrix. The load-time curve for a specimen that was aged for 10,000 h exhibits a sudden drop in load, indicating a brittle fracture mode. Such load-time curves were typical of all heats containing >20% ferrite.

The Charpy-impact data for some of the heats of cast stainless steel are presented in Figs. 2-5 and compared with the results from studies by Georg Fischer Co., Switzerland (GF)[4] and Framatome, France (FRA).[7] The chemical composition and the ferrite content of the various materials are given in Table 1. The different temperatures and times for aging were normalized in terms of the parameter P, by means of Eqs. (1) and (2). The service time at 320°C is also shown in each figure. The significant results are as follows.

(a) The time-temperature correlations given in Eqs. (1) and (2) are valid for each of the three GF heats of material, i.e., the data for aging temperatures of 300, 350, and 400°C can be represented by a single correlation between impact energy and parameter P. The impact energy for Heat 286 aged at 400°C for relatively short times (i.e., P <2.5) is slightly lower than that for the material aged at 350 or 300°C, Fig. 4a. Table 1 shows that the carbon content in Heat 286 is significantly higher than in Heats 280 or 278. The results also indicate

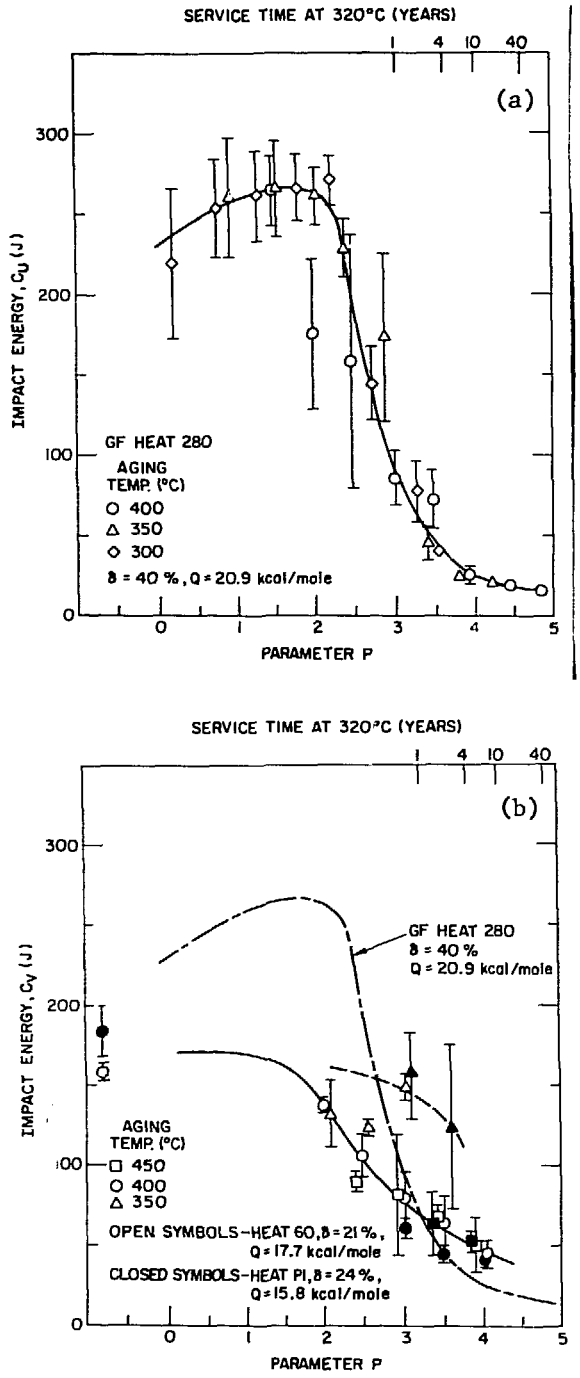

Fig. 2. Influence of Thermal Aging on the Room-Temperature Impact Energy of CF-8 and -3 Cast Stainless Steel. (a) Georg Fischer (GF) Heat 280 (Ref. 4) and (b) Heats 60 and P1.

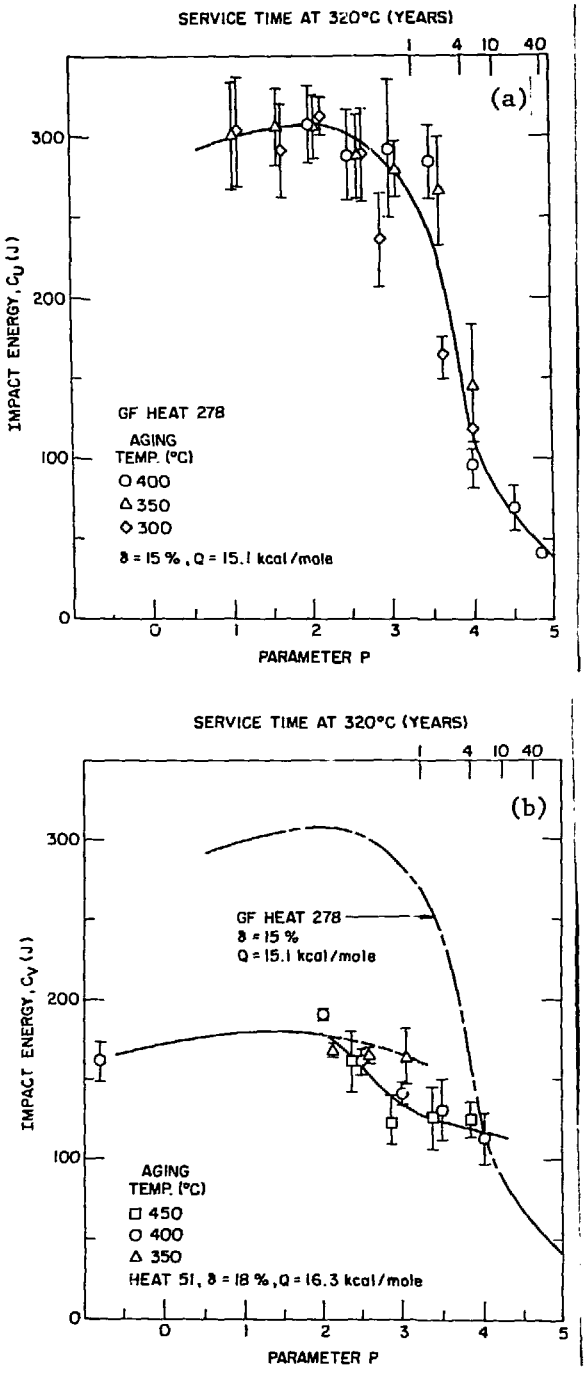

Fig. 3. Influence of Thermal Aging on the Room-Temperature Impact Energy of CF-8 and -3 Cast Stainless Steel. (a) Georg Fischer (GF) Heat 278 (Ref. 4) and (b) Heat 51.

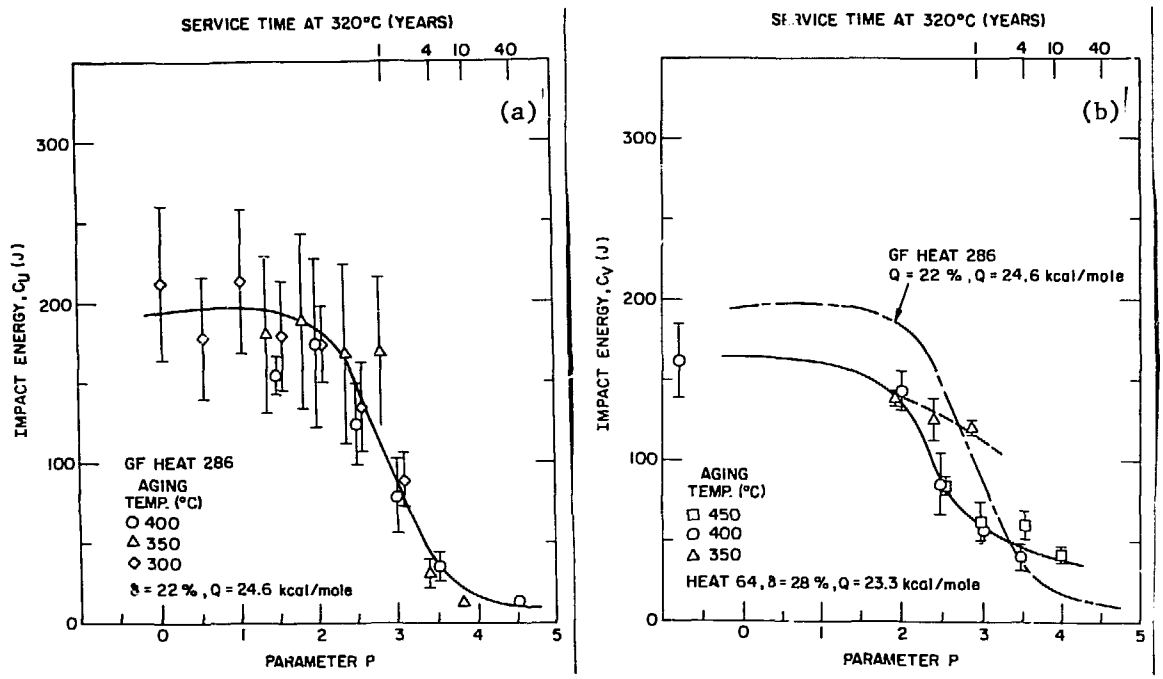

Fig. 4. Influence of Thermal Aging on the Room-Temperature Impact Energy of CF-8M Cast Stainless Steel. (a) Georg Fischer (GF) Heat 286 (Ref. 4) and (b) Heat 64.

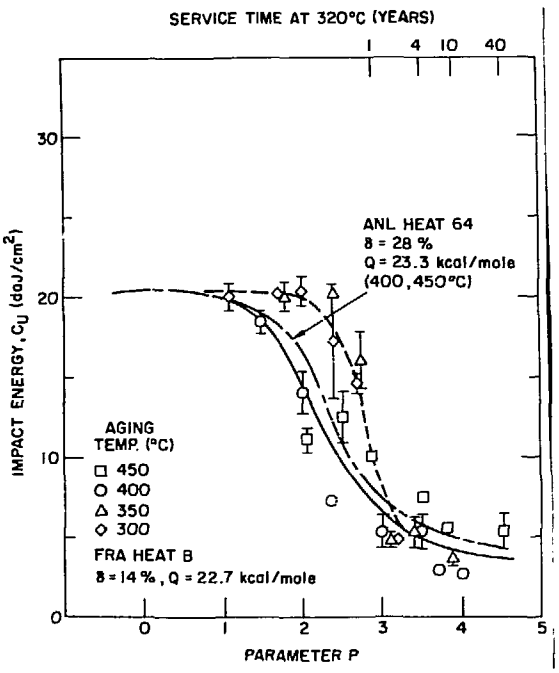

Fig. 5.
Influence of Thermal Aging on the Normalized Impact Energy at Room Temperature for CF-8 Cast Stainless Steel (Ref. 7).

Table 1. Chemical Composition and Ferrite Content of Cast Stainless Steel

Heat	Chemical Composition, wt %							Ferrite Content, %	
	Si	Mn	Ni	Cr	Mo	C	N	Calculated[a]	Measured[b]
Experimental Heats									
60	1.01	0.71	8.07	21.02	0.26	0.070	0.050	16.9	21
51	1.06	0.66	8.69	20.36	0.28	0.023	0.048	17.5	18
64	0.71	0.70	9.01	20.87	2.41	0.050	0.030	32.2	28
Commercial Heat									
P1	1.07	0.56	8.10	20.49	0.04	0.032	0.053	18.8	24
Pump Cover Plate from KRB Reactor[c]									
KRB	1.17	0.31	8.03	21.99	0.17	0.062	0.038	27.7	26
Georg Fischer Heats[d]									
280	1.37	0.50	8.00	21.60	0.25	0.028	0.029	38.6	40
278	1.00	0.28	8.27	20.20	0.13	0.038	0.027	19.0	15
286	1.33	0.40	9.13	20.20	2.44	0.072	0.063	18.7	22
Framatome Heat[e]									
B	0.93	0.83	10.56	20.12	2.52	0.053	0.042	14.0	-

[a]Calculated from chemical composition with Hull's equivalent factor.
[b]Measured by ferrite scope (Auto test FE, Probe Type FSP-1).
[c]The material was in service for ~12 yr at 284°C. A 75% capacity factor is assumed.
[d]Fractured Charpy-impact bars were obtained from Georg Fischer Co., Switzerland, for microstructural evaluation. Charpy-impact test data from Ref. 4.
[e]Charpy-impact test data from Ref. 7.

that the time for the onset of embrittlement is different for the different materials, e.g., ~2 yr service at 320°C for Heat 278 and <1 yr service at 320°C for Heats 280 and 286.

(b) The data for the materials used in the present investigation and for FRA Heat B do not follow a single curve. The impact energy for the materials aged at 450 and 400°C decreases much more rapidly than for the materials aged at 350 or 300°C, i.e., the onset of embrittlement is sooner for materials aged at 450 and 400°C than for those aged at lower temperatures. The difference between high- and low-temperature data is greater for Heats 60, P1, 64, and B containing >0.05 wt % C relative to Heat 51 with ~0.02 wt % C. Results for FRA Heat B indicate that the impact energies are comparable for material aged at high or low temperatures for long times, Fig. 5.

(c) The impact energies of the unaged GF heats are significantly higher than those for the other heats. This difference may be attributed to the unique heat treatment of the materials. The GF heats were reheat-treated in the laboratory after the commercial heat treatment, while the other heats were in the commercial heat-treated condition. The room-temperature impact energies of the unaged GF heats probably correspond to the upper shelf energy, whereas the values for the other heats represent the ductile-to-brittle transition.

(d) After 10,000 h aging at 400°C, the low-carbon Heat 51 shows a relatively small reduction in impact energy compared to other heats with higher carbon but a comparable ferrite content. For example, the impact energy decreases by ~30% for Heat 51 containing 18% ferrite, whereas Heat 60 with 21% ferrite and GF Heat 278 with 15% ferrite show a reduction in impact strength of >70%.

The change in impact energy of cast CF-8 stainless steel after reactor service is shown in Fig. 6. The specimens were obtained from the KRB pump cover plate which was in service for ~12 yr at a nominal temperature of 284°C. The actual temperature of the test material ranged between 265 and 278°C. The impact energies of the KRB material are slightly higher than those predicted by the average curve for GF Heat 280 or the Argonne Heat 60.

These results indicate that the activation energies obtained from Eq. (2) do not accurately represent the embrittlement behavior of cast stainless steels over the entire temperature range of 300 to 450°C. The carbon content in the steel appears to play an important role in the overall process of embrittlement. The rapid decrease in impact energy during high-temperature aging, i.e., at 400 and 450°C, is most likely caused by the precipitation of carbides in the ferrite matrix or at the ferrite/austenite boundary. Such processes either do not occur or are too slow at lower temperatures, and the embrittlement of the steel is primarily caused by the formation of other phases, such as α' or G phase.

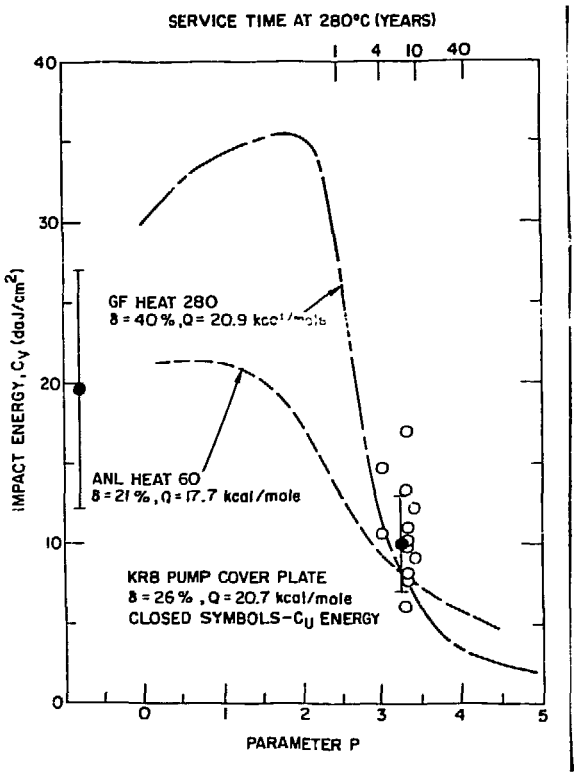

Fig. 6.
Normalized Impact Energy at Room Temperature for CF-3 Cast Stainless Steel after ~12-yr Service at ~284°C.

Figure 7 shows the influence of thermal aging on the impact energy and microhardness of the ferrite phase for Heat 51 (grade CF-3) and Heat 60 (grade CF-8). The results indicate that the impact energy decreases and the microhardness of the ferrite phase increases with aging time. For a given aging condition, the microhardness of the ferrite is comparable for Heats 51 and 60. However, the reduction in impact energy is significantly higher for Heat 60 than for Heat 51. Microstructural characteristics of Heats 51 and 60, discussed in the next section, suggest that the difference in impact strength arises from the precipitation of carbides at the ferrite/austenite phase boundaries in Heat 60.

4. Microstructural Characterization

Microstructures of the aged and fractured impact test specimens were characterized by TEM, SEM, optical microscopy, and small-angle neutron scattering (SANS) techniques. The results of a microstructural examination of the GF materials and the KRB pump cover plate have been reported previously,[8,13,14] The microstructural characteristics were correlated with the fracture behavior of the impact specimens to provide a better understanding of the embrittling mechanism(s) of cast-duplex stainless steels.[14] The results showed that three phases were responsible for the embrittlement of the ferrite phase. Precipitation on the ferrite/austenite phase boundary was also identified and was found to be responsible for the weakening of the phase boundary.

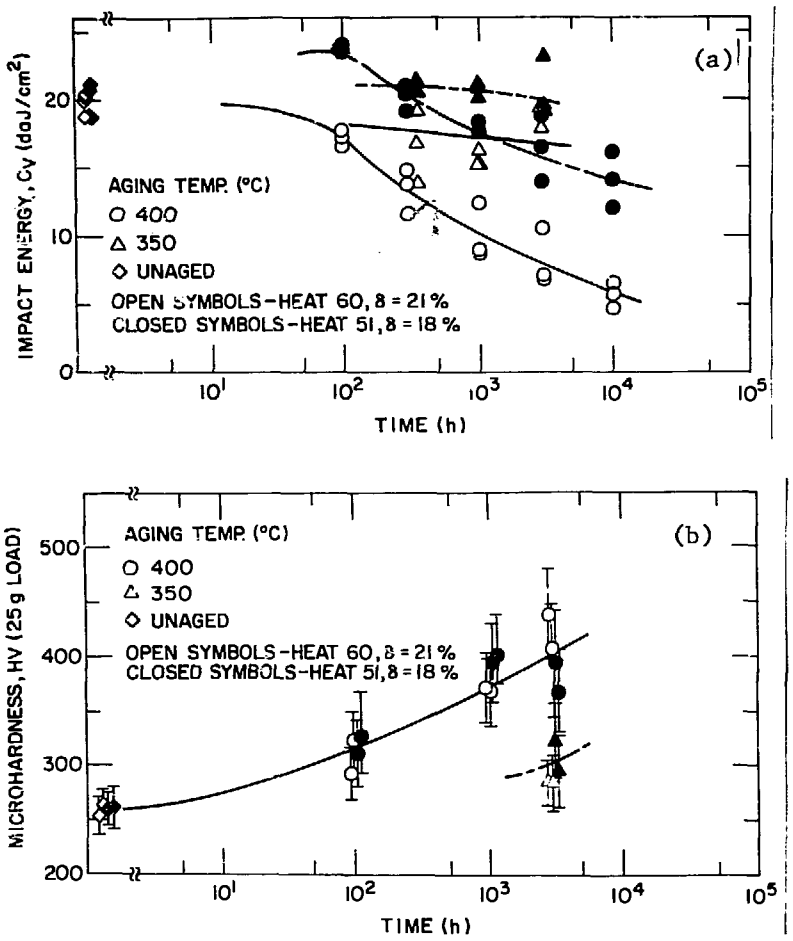

Fig. 7. Influence of Thermal Aging on the (a) Room-Temperature Impact Energy and (b) Microhardness of the Ferrite Phase for CF-3 (Heat 51) and CF-8 (Heat 60) Grades of Cast Stainless Steel.

4.1 Embrittlement of the Ferrite Phase

The characteristics of the three precipitates, i.e., G-phase, Type X, and the chromium-rich α', can be summarized as follows:

G-Phase

Figure 8 shows the characteristic morphology and selected-area diffraction (SAD) patterns of the G-phase observed in the GF material after aging at 400°C for 7.6 yr. The precipitates were also observed in the reactor-aged pump cover material, which was exposed to the coolant at ~274°C for ~12 yr. Volume fractions of the G-phase in the KRB pump material or in GF Heats 280 and 278, aged at 300°C for ~8 yr (Figs. 2 and 3), were not large enough to produce distinct reflections in the diffraction patterns [similar to those of

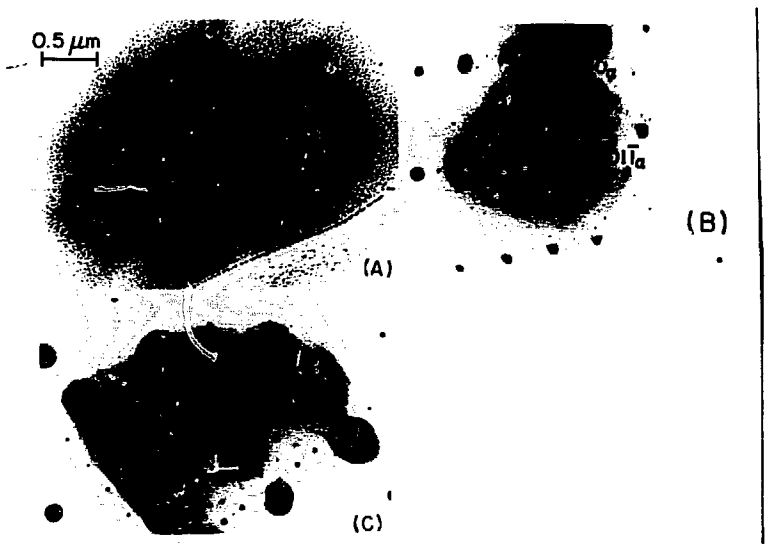

Fig. 8. Dark-Field Morphology (A) and Characteristic SAD Patterns (B and C) of the Ni- and Si-rich G-Phase Observed in CF-8 Cast-Duplex Stainless Steel after Aging at 400°C for 7.6 yr.

Figs. 8(B) and (C)]. Although 400°C aging produced precipitates of the G-phase in the ferrite grains as well as on the grain boundaries [Fig. 8(A)], no grain boundary precipitation was observed after aging at ≤300°C. During lower temperature aging, the precipitates were observed primarily in association with dislocations in the ferrite; this observation indicates a dislocation pinning effect. The nearly spherical precipitate is ~5 nm in size. The diffraction patterns are similar to those of the $M_{23}C_6$ phase, but with a slightly larger lattice parameter. The precipitates also had a cube-on-cube orientation relative to the bcc ferrite matrix, which would be unusual for the $M_{23}C_6$ phase. (400) reflections were characteristically weak or absent in the diffraction patterns [Fig. 8(C)]. Energy-dispersive x-ray analysis showed an enrichment of Ni and Si in the precipitates. From these results, the precipitates were identified as the G-phase (a phase rich in Ni and Si), which has been observed in an Fe-12Cr-4Ni alloy after aging at 450°C[15] and in commercial EM-12 (9Cr-2Mo), HT-9 (12Cr-1Mo), and AISI 416 (13Cr) ferritic steels after irradiation at temperatures of <425°C.[16]

Type X Precipitates

In both the KRB pump material and GF Heats 280 and 278, aged at 300°C for 8 yr, the unidentified (Type X) precipitate was always observed on dislocations. Figure 9 shows the morphology of the precipitates observed in the KRB pump material that are interwoven with the dislocations. Apparently, the precipitates were very effective in pinning dislocation motion in the material aged for a long time near 300°C. The precipitate reflections in the SAD

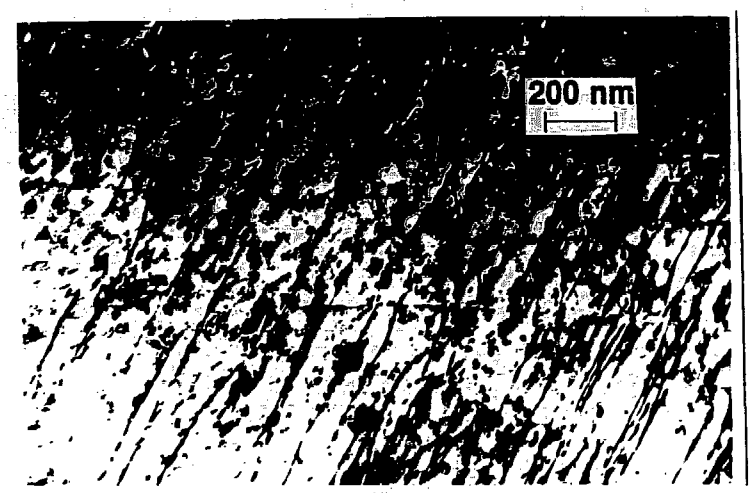

Fig. 9. Dark-Field Image Showing Light Type X Precipitates Interwoven with Dislocations in the Ferrite Phase of the Reactor Pump Cover Material.

patterns were weak, diffuse, and streaked, owing to a low volume fraction and small particle size. In typical SAD patterns containing the Type-X precipitates, only extremely weak precipitate reflections with a d-spacing of 0.218 nm were detected. The weak reflections could not be detected on the microscope screen. No cross-grid patterns could be obtained.

α' Precipitate

Chromium-rich α' precipitates in the ferrite were observed in KRB pump-cover material, Fig. 10(A). The extremely small (1-2 nm) α' precipitates could not be resolved by TEM either under a strong bright-field or under a dark-field imaging condition. The precipitates could be resolved only under a weak-beam bright-field imaging condition. The mottled morphology characteristic of the α' was difficult to resolve in the GF material after aging at 300°C for 8 yr. However, optimum weak-beam imaging[17] at a magnification of 20-40 thousand times revealed α' precipitates 1-1.5 nm in size when the negatives were developed and examined on a lighted table with a magnifying glass. Negatives taken under normal bright- or dark-field imaging condition did not reveal any α' precipitates in the GF materials. Figure 10(B) shows the α' in the ferrite of Heat 60 after aging at 400°C for 1.2 yr. The α' size and morphology are similar to those of the KRB reactor-aged material.

4.2 Precipitate Characterization by Small-Angle Neutron Scattering

Although the very fine α' in the GF materials, aged either at 300°C for 8 yr or at 400°C for 7.6 yr, could be resolved by the weak-beam TEM technique, the results from the small-angle neutron scattering experiments showed no

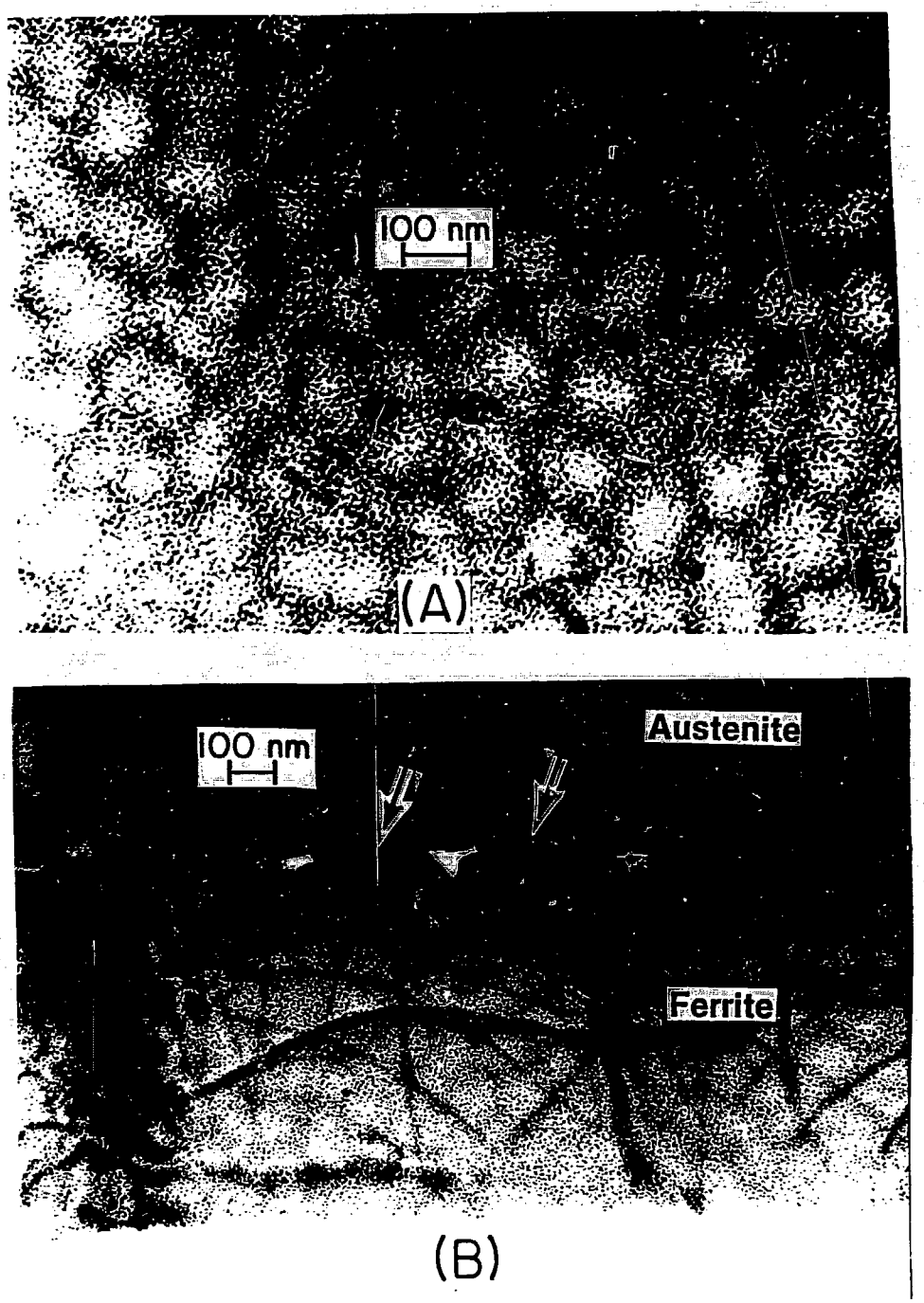

Fig. 10. Morphologies of α' Observed in the Ferrite Phase of the Reactor Pump Cover (A) and Heat 60 Cast-Duplex Stainless Steel after Aging at 400°C for 10,000 h (B). $M_{23}C_6$ precipitates on the phase boundary are denoted by arrows in (B).

distinct intensity peak at ~1-nm diameter, which corresponds to the size of α' in the materials. However, an intensity peak corresponding to the G-phase, which exhibits a distinct phase boundary (relative to the ferrite matrix) and a size an order of magnitude larger than the α', was observed as shown in Fig. 11.[18] The diameters of the most populous scattering centers shown in Figs. 11(A) and (B), i.e., ~1.6 and ~5.5 nm, are in good agreement with the sizes of the G-phase observed by TEM for the two aging conditions, i.e., GF Heat 278 aged at 400°C for 1.2 and 7.8 yr, respectively. A comparison of Figs. 11(A) and (B) shows an Ostwald ripening of the G-phase after aging at 400°C for 7.6 yr. The absence of an intensity peak corresponding to the α' size (1-2 nm) in Fig. 11 is not surprising since a distinct phase boundary is not expected between the chromium-rich α' and chromium-depleted ferrite phase in the materials.

4 3 Grain Boundary Precipitate

A distinct difference between the microstructures of the laboratory-aged GF materials and the reactor pump-cover material involves precipitation of a grain boundary phase in the latter. Bright- and dark-field morphologies and an SAD pattern of the grain boundary phase are shown in Fig. 12. The phase was observed on the boundary between the austenite and ferrite grains, examples of which appear as the dark and light areas, respectively, in Fig. 12(A). Several different zone axes similar to that of the SAD pattern in Fig. 12(C) were obtained. Indexing of the diffraction patterns showed that the grain boundary precipitates were $M_{23}C_6$ carbides, which were of cube-on-cube orientation relative to austenite. The overall distribution of the grain boundary phase could be more clearly observed in low-magnification optical micrographs. For example, in Fig. 12(D), ~60% of the austenite-ferrite grain boundaries are decorated by the phase; this observation indicates a possible weakening of the grain boundaries. The lacy morphology of the ferrite is evident from Fig. 12(D). Aging of Heat 60 also yielded grain boundary precipitation of the $M_{23}C_6$ carbide, Fig. 10(B). The chemical composition of Heat 60 is very similar to that of the reactor pump material. However, the grain boundary $M_{23}C_6$ carbide was not observed in the low-carbon Heat 51 after aging at 400°C for ~1.2 yr. The absence of grain-boundary carbide precipitates in Heat 51 and the GF materials, i.e., Heats 280 and 278, is most likely related to the low-carbon contents (Table 1) compared to the higher carbon contents of the reactor pump and Heat 60 materials.

The precipitation of grain boundary carbides appears to be responsible for the rapid reduction in the impact energy for the high-carbon Heat 60 compared to that for Heat 51 [Fig. 7(a)]. However, the microstructural characteristics of the ferrite matrix are similar for the two heats and, as expected, the hardnesses of the ferrite phase are comparable [Fig. 7(b)]. The grain-boundary $M_{23}C_6$ precipitation in Heat 60 was significantly smaller after aging at 350°C for 10,000 h than after aging at 400°C for similar times. This is believed to be one of the factors which contribute to the higher impact

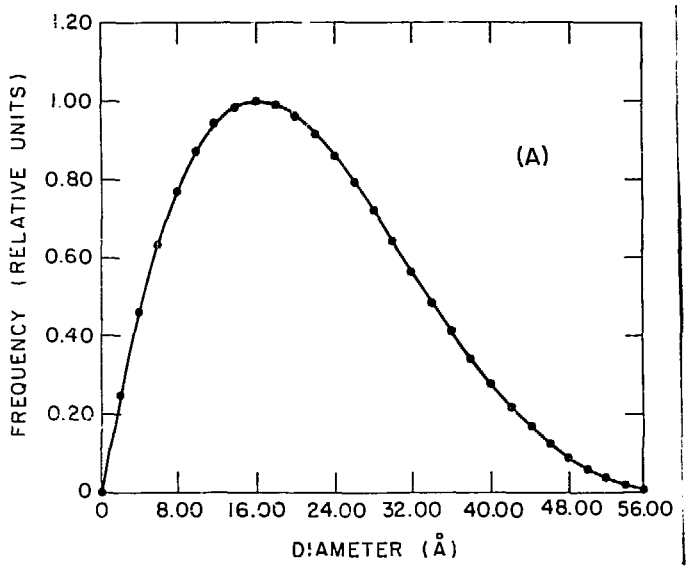

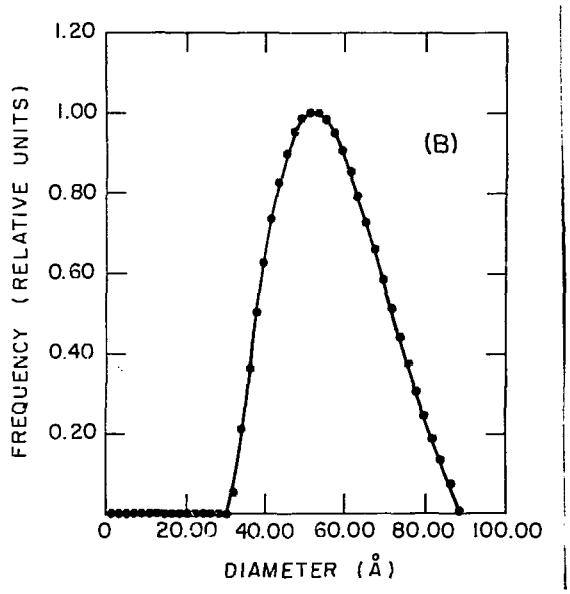

Fig. 11. Relative Population of Precipitates vs Guinier Diameter Obtained by Small-angle Neutron Scattering Technique for the G. Fischer Cast-Duplex Stainless Steel Heat 278 after Aging at 400°C for 1.2 yr (A) and 7.6 yr (B).

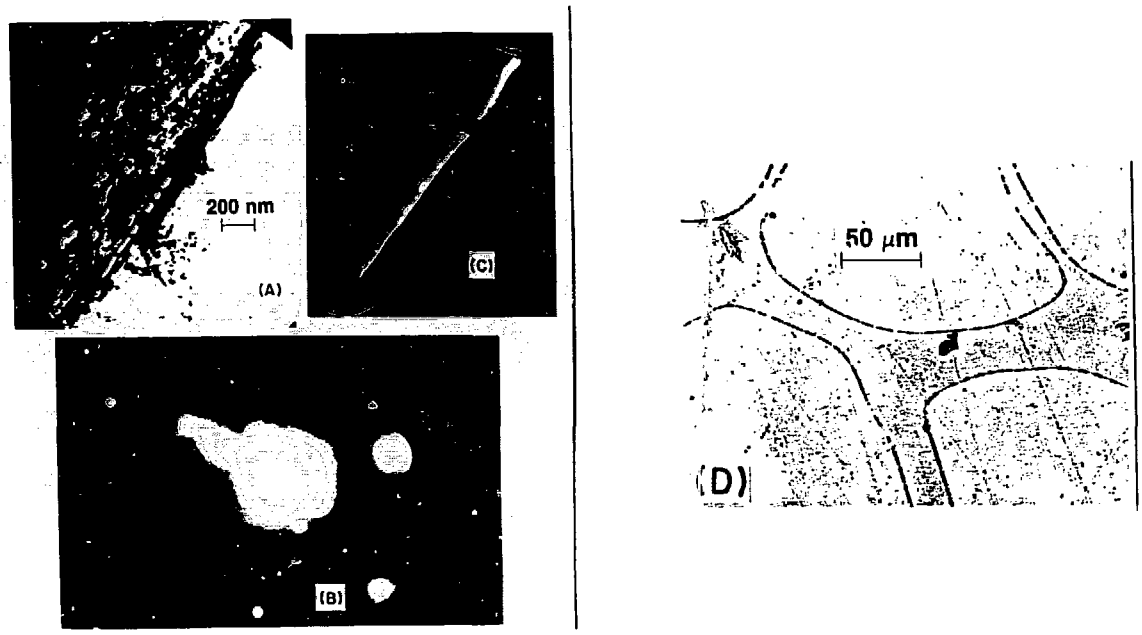

Fig. 12. Bright-Field (A) and Dark-Field (B) Images, SAD Pattern (C), and an Optical Micrograph (D) of $M_{23}C_6$ Grain Boundary Precipitates Observed in the Reactor Pump Cover Material.

energies for Heat 60 aged at 350°C relative to those aged at higher temperatures. However, the lower hardness of the ferrite phase for the material aged at 350°C indicates that other factors, viz., microstructural characteristics of the ferrite matrix, also contribute to the overall embrittlement behavior.

4.4 SEM Fractography

Fracture surface morphologies of the laboratory-aged GF materials and the reactor pump-cover material were evaluated by SEM after room-temperature impact tests. The fracture surface morphology of the ferrite phase of the reactor pump cover and the GF material aged at 300°C for 8 yr or at 400°C for 1.2 yr was invariably cleavage-type (Fig. 13), which means negligible ductility of the phase. Undoubtedly, the ferrite was generally embrittled by one or combinations of the above-mentioned precipitates, i.e., G-phase, Type X, and α'. It was, in fact, possible to map the cleavage-ferrite and ductile-austenite portions of a given fracture surface. The cleavage map of the reactor pump cover indicated that ~50-60% of the overall fracture surface was ferrite, although the ferrite volume fraction was only ~30%. Although not conclusive, this finding indicates preferential crack propagation along the ferrite phase under the impact condition. There was also some indication of decohesion along the grain boundary of the reactor pump-cover material, as shown in Fig. 13(B). The relatively smooth morphology shown in Fig. 13(B) appears to correspond to grain boundaries that are partly covered by ductile

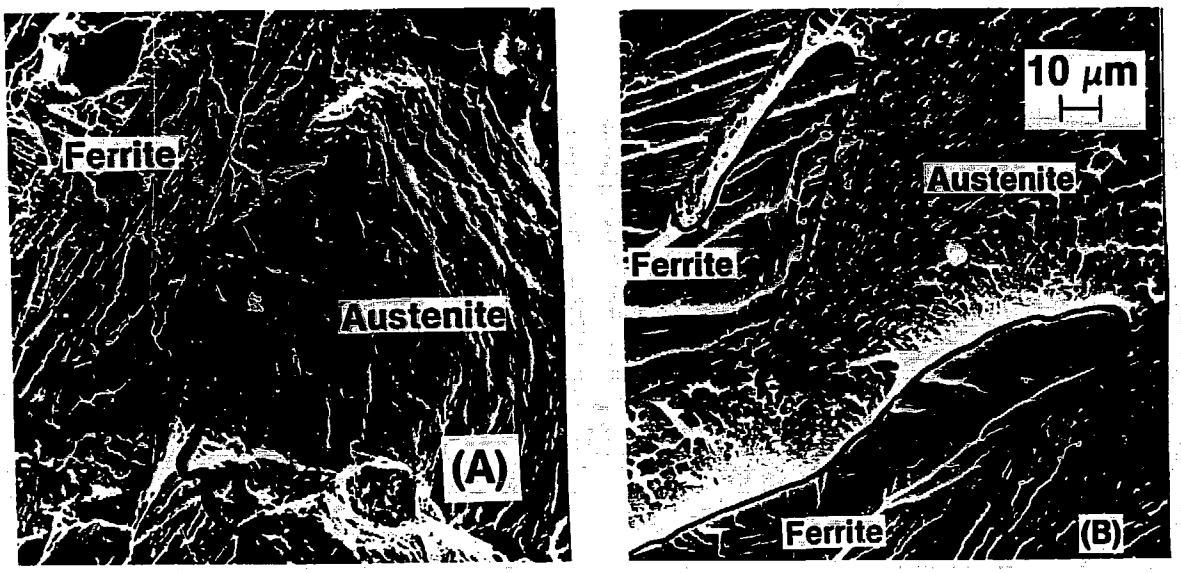

Fig. 13. Fracture Surface Morphologies of the Room-Temperature Impact-tested Specimens of the G. Fischer Material Aged at 300°C for 8 yr (A) and the Reactor Pump Cover Material after 12 yr of Service in a Boiling-Water Reactor (B).

tears. This observation is consistent with the microstructures of Fig. 12, in which a significant fraction of the grain boundaries was covered by the carbide precipitates. However, for the laboratory-aged GF materials, the austenite fracture surface morphology invariably showed transgranular ductile failures, as in Fig. 13(A).

5. Conclusions

Data from room-temperature impact tests and microstructural characterization indicate that the existing correlations do not accurately represent the embrittlement behavior of cast-duplex stainless steels over the temperature range of 300-450°C. The carbon content in the steel may be an important factor in controlling the overall process of embrittlement, particularly at temperatures $\geq$400°C. Preliminary results suggest that at least two processes contribute to the embrittlement of duplex stainless steels, viz., weakening of the ferrite/austenite phase boundary by carbide precipitation, and embrittlement of ferrite matrix by the formation of additional phases such as G-phase, Type X, or the α' phase. The latter occurs in all heats of cast stainless steels and is primarily responsible for embrittlement of low-carbon materials (i.e., CF-3 grade) at temperatures below 350°C. However, the relative importance of the three precipitates under different compositional and aging conditions cannot be quantitatively established at this time. The precipitation of $M_{23}C_6$ carbides at the ferrite/austenite phase boundary has a significant effect on embrittlement of high-carbon materials, i.e., grade CF-8.

Carbide precipitation dominates the onset of embrittlement of cast CF-8 or -8M stainless steels aged at 400 or 450°C. Charpy-impact and microstructural data will be obtained on materials aged at temperatures between 290 and 350°C for long times to evaluate the relative contribution of the different precipitation processes on embrittlement of cast-duplex stainless steels.

6. Acknowledgments

The authors acknowledge the experimental contributions provided by L. P. Burkel and metallography and scanning electron microscopy performed by R. A. Conner, Jr. and G. M. Dragel. This work was supported by the U. S. Nuclear Regulatory Commission, Office of Nuclear Regulatory Research, under Contract W-31-109-Eng-38. The authors wish to thank W. J. Shack and J. Muscara for their helpful discussions.

References

1. H. D. Solomon and T. M. Devine, "Influence of Microstructure on the Mechanical Properties and Localized Corrosion of a Duplex Stainless Steel," in Micon 78: Optimization of Processing, Properties, and Service Performance Through Microstructural Control, eds. Abrams, Maniar, Nail, and Solomon, ASTM STP 672 (1979), p. 430.

2. P. J. Grobner, "The 885°F (475°C) Embrittlement of Ferritic Stainless Steels," Metall. Trans. 4 (1973), p. 251.

3. T. J. Nichol, A. Dalta, and G. Aggen, "Embrittlement of Ferritic Stainless Steels," Metall. Trans. 11A (1980), p. 573.

4. A. Trautwein and W. Gysel, "Influence of Long Time Aging of CF-8 and CF-8M Cast Steel at Temperatures Between 300 and 500 deg. C on the Impact Toughness and the Structure Properties," Spectrum, Technische Mitteilungen aus dem+GF+Konzern, No. 5 (May 1981); Stainless Steel Castings, eds. V. G. Behal and A. S. Melilli, ASTM STM 756 (1982), p. 165.

5. G. Baudry and C. Pichard, "Evolution During Long Holding Times at 300 and 450°C of the Mechanical Properties of Austeno-Ferritic Steel Castings and Welded Joints Used in Pressurized Water Nuclear Reactors," in Troisieme Congres National Sur La Technologie Des Appareils a Bression, Vol. 2, Materiaux, A.F.I.A.P. (1980), p. 673.

6. E. I. Landerman and W. H. Bamford, "Fracture Toughness and Fatigue Characteristics of Centrifugally Cast Type 316 Stainless Steel Pipe after Simulated Thermal Service Conditions, Ductility, and Toughness Considerations in Elevated Temperature Service," ASME MPC-8 (1978), p. 99.

7. G. Slama, P. Petrequin, and T. Magep, "Effect of Aging on Mechanical Properties of Austenitic Stainless Steel Castings and Welds," presented at SMIRT Post-Conference Seminar 6, Assuring Structural Integrity of Steel Reactor Pressure Boundary Components, August 29 and 30, 1983, Monterey, CA.

8. O. K. Chopra and G. Ayrault, "Aging Degradation of Cast Stainless Steel: Status and Program," Nucl. Eng. Des. 86 (1985), p. 69.

9. O. K. Chopra and H. M. Chung, "Aging of Cast Duplex Stainless Steels in LWR Systems," in Proc. of the U. S. Nuclear Regulatory Commission Twelveth Water Reactor Safety Research Information Meeting, NUREG/CP-0058 Vol. 4 (1985), p. 211.

10. M. K. Miller, J. Bentley, S. S. Brenner, and J. A. Spitznagel, "Long Term Thermal Aging of Type CF-8 Stainless Steel," J. Phys. (Paris) Colloq. 45 (1984), p. C9-385.

11. J. Bentley, M. K. Miller, S. S. Brenner, and J. A. Spitznagel, "Identification of G Phase in Aged Cast CF-8 Type Stainless Steel," in Proc. of the 43rd Annual Meeting of the Electron Microscopy Society of America, G. W. Bailey, ed. (1985), p. 328.

12. O. K. Chopra and G. Ayrault, in Materials Science and Technology Division Light-Water-Reactor Safety Research Program: Quarterly Progress Report, October-December 1983, NUREG/CR-3689 Vol. IV, ANL-83-85 Vol. IV (August 1984), pp. 129-151.

13. O. K. Chopra and H. M. Chung, in Materials Science and Technology Division Light-Water-Reactor Safety Materials Engineering Research Programs: Quarterly Progress Report, January-March 1984, NUREG/CR-3998 Vol. I, ANL-84-60 Vol. I (September 1984), p. 52.

14. H. M. Chung and O. K. Chopra, "Microstructure of Cast-Duplex Stainless Steel after Long-Term Aging," in Proc. Second Intl. Symp. on Environmental Degradation of Materials in Nuclear Power Systems - Water Reactors, September 9-12, 1985, Monterey, CA, to be published.

15. G. T. Brown and R. T. Allsop, "Embrittlement of a 12%Cr-4Ni Steel," J. Iron Steel Inst. (1960), p. 435.

16. D. S. Gelles and L. E. Thomas, "Effects of Neutron Irradiation on Microstructure in Commercial and Experimental Ferritic Alloys," presented at Topical Conf. on Ferritic Alloys for Use in Nuclear Energy Technologies, June 19-23, 1983, Snowbird, UT.

17. D. J. H. Cockayne, "The Weak-Beam Method of Electron Microscopy," in Diffraction and Imaging Techniques in Material Science, S. Amelinckx, R. Gevers, and J. Van Landuyt, eds., North Holland, 1978, Vol. I, pp. 153-183.

18. J. E. Epperson, J. S. Lin, and S. Spooner, "The Fine Scale Microstructure in Cast and Aged Duplex Stainless Steels Investigated by Small Angle Neutron Scattering," to be published.